(2)

TRANSIENT INTERNAL PROBE DIAGNOSTIC

Annual Technical Report #1
(9-15-90/10-14-91)
Grant No. AFOSR-90-0345

by

Thomas R. Jarboe (P.I.)
Gregory G. Spanjers
Walter H. Christiansen
Glen A. Wurden
Bradford L. Wright

Original contains color plates: All DTIC reproductions will be in black and white

University of Washington
Aerospace & Energetics Research Program
Seattle, Washington 98195

submitted: December 12, 1991

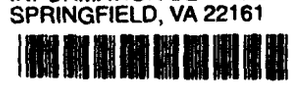

unclassified

SECURITY CLASSIFICATION OF THIS PAGE

REPORT DOCUMENTATION PAGE

1a. REPORT SECURITY CLASSIFICATION: unclassified	1b. RESTRICTIVE MARKINGS
2a. SECURITY CLASSIFICATION AUTHORITY	3. DISTRIBUTION/AVAILABILITY OF REPORT: ~~n/a~~ unlimited
2b. DECLASSIFICATION/DOWNGRADING SCHEDULE	
4. PERFORMING ORGANIZATION REPORT NUMBER(S)	5. MONITORING ORGANIZATION REPORT NUMBER(S)
6a. NAME OF PERFORMING ORGANIZATION: Aerospace & Energetics Research Program; 6b. OFFICE SYMBOL (If applicable): FL-10	7a. NAME OF MONITORING ORGANIZATION: Air Force Office of Scientific Research
6c. ADDRESS (City, State and ZIP Code): University of Washington, Seattle, Washington 98195	7b. ADDRESS (City, State and ZIP Code): Bolling Air Force Base, D.C. 20332-6448
8a. NAME OF FUNDING/SPONSORING ORGANIZATION: AFOSR; 8b. OFFICE SYMBOL (If applicable): /NP	9. PROCUREMENT INSTRUMENT IDENTIFICATION NUMBER: AFOSR-90-0345
8c. ADDRESS (City, State and ZIP Code): Building 410, Bolling Air Force Base, D.C. 20332-6448	10. SOURCE OF FUNDING NOS.

PROGRAM ELEMENT NO.	PROJECT NO.	TASK NO.	WORK UNIT NO.
61102F	2301	A8	

11. TITLE (Include Security Classification): (unclassified) TRANSIENT INTERNAL PROBE DIAGNOSTIC

12. PERSONAL AUTHOR(S): JARBOE, Thomas R.; SPANJERS, Gregory G.; CHRISTIANSEN, Walter H.; WURDEN, Glen A.; WRIGHT, Bradford L.

13a. TYPE OF REPORT	13b. TIME COVERED	14. DATE OF REPORT (Yr., Mo., Day)	15. PAGE COUNT
annual technical rpt	FROM 90/9/15 TO 91/10/14	1991 December 12	44

16. SUPPLEMENTARY NOTATION: n/a

17. COSATI CODES		
FIELD	GROUP	SUB. GR.

18. SUBJECT TERMS (Continue on reverse if necessary and identify by block number): transient internal probe; magnetic fusion diagnostic; Verdet material; Faraday rotator material; polarization measurements; 2-stage light gas gun; diamond ablation

19. ABSTRACT (Continue on reverse if necessary and identify by block number)

The Transient Internal Probe (TIP) diagnostic is a novel method for probing the interior of hot magnetic fusion plasmas that are inaccessible with ordinary stationary probes, by limiting the time that the probe is in the plasma, and by encasing the probe in a diamond cladding. In the TIP scheme, a probe is fired through a hot plasma at velocities in excess of 2.5 km/s, and makes direct, local measurements of the internal magnetic field structure. These measurements are relayed to the laboratory optical detection system, using an incident laser that is retroreflected through a Faraday rotator crystal payload that acts as a magneto-optic sensor.

The individual tasks associated with the TIP development, construction of a two-stage light gas gun, optical detection system and probe projectile, are currently being completed. Integration of these tasks is currently underway. It is expected that the integrated system will be functional in the first six months of 1992. A diamond ablation study has also been performed to measure the ablative effects of a hot plasma in contact with a diamond pellet.

Studies are currently underway to develop a sabot stripping system, and to develop a vacuum interface system between the TIP diagnostic and the plasma experiments' vacuum chamber.

20. DISTRIBUTION/AVAILABILITY OF ABSTRACT	21. ABSTRACT SECURITY CLASSIFICATION
UNCLASSIFIED/UNLIMITED ☒ SAME AS RPT. ☐ DTIC USERS ☐	unclassified

22a. NAME OF RESPONSIBLE INDIVIDUAL	22b. TELEPHONE NUMBER	22c. OFFICE SYMBOL
Barker	202-767-5011	NE

DD FORM 1473, 83 APR EDITION OF 1 JAN 73 IS OBSOLETE.

unclassified

SECURITY CLASSIFICATION OF THIS PAGE

DISCLAIMER NOTICE

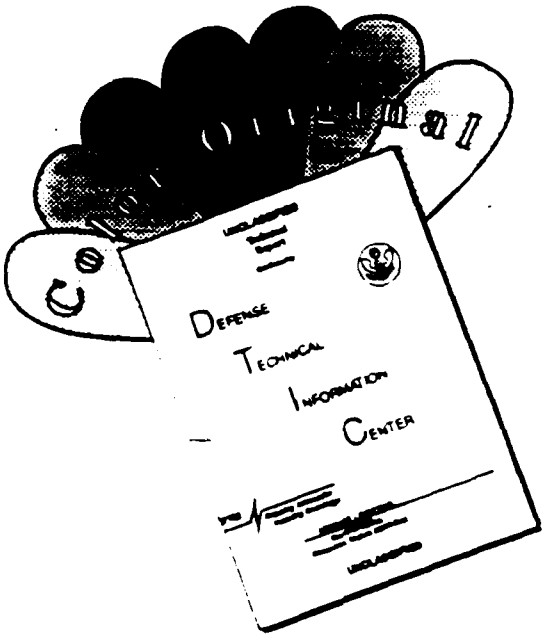

THIS DOCUMENT IS BEST QUALITY AVAILABLE. THE COPY FURNISHED TO DTIC CONTAINED A SIGNIFICANT NUMBER OF COLOR PAGES WHICH DO NOT REPRODUCE LEGIBLY ON BLACK AND WHITE MICROFICHE.

SUMMARY

This report presents a summary of the work performed during Year 1 (9/15/90 - 10/15/91) for the Transient Internal Probe Diagnostic (TIP) experiment at the University of Washington, Seattle. This work has been performed under the Air Force Office of Scientific Research Grant #AFOSR-90-0345.

The TIP diagnostic is a novel method for probing the interior of hot magnetic fusion plasmas that are inaccessible with ordinary stationary probes. In the TIP scheme, a probe is fired through a hot plasma at velocities in excess of 2.5 km/s, and makes direct, local measurements of the internal magnetic field structure. These measurements are relayed to the laboratory using an incident laser that is retroreflected through a Faraday rotator crystal payload that acts as a magneto-optic sensor.

In the initial stages, the TIP program consists of three independent tasks which, after completion, are integrated to form a cohesive unit. These three tasks are: (1) The construction of a diamond projectile with a Faraday rotator crystal payload that serves as a magneto-optic sensor, (2) The construction of a laser-detector system to beam laser light to the transient probe and measure the local magnetic field at the projectile's position from the rotation of the plane of polarization of the retroreflected light, and (3) The construction of a two-stage light gas gun to fire the projectile, along with the development of a sabot, a sabot stripper, and a vacuum interface with a plasma device. Also added to the TIP development was, (4) A diamond ablation study necessary to determine the ablative effects of a hot plasma in contact with the diamond-clad projectile. As a proof-of-principle of the TIP concept, the integrated unit will ultimately be used to make internal magnetic field measurements on the Helicity Injected Torus (HIT) at the University of Washington.

At the completion of Year 1, the status of the TIP development is as follows:

(1) The design for the magneto-optic crystal probe has been optimized through the use of ray tracing programs that calculate the correct probe dimensions that correctly focus the retroreflected laser light to achieve the maximum beam intensity at the laser detection system. The design is a two-piece probe consisting of a microlens attached to a Faraday rotator crystal cylinder, with the length of the cylinder calculated to be slightly less than the effective focal length. Methods have been developed and tested for fabricating and optically polishing the probe material. Final fabrication of the probe is ready and will be performed following a

laboratory investigation of the optical detection system sensitivity.

(2) The design and construction of the optical detection system is complete. It has been found that the use of three photodetectors behind polarized filters at different angles minimizes the error of the polarization measurement and eliminates the effects of retroreflected laser intensity and background light intensity. Presently, the optical detection system is being calibrated for polarization angle measurements.

(3) The design of the two-stage light gas gun is complete. Each of the individual components (gun barrel, pump tube, gas reservoir, connecting flanges and diaphragms) is either fabricated or will be completed within 30 days. Presently the individual components are being hydrostatically tested and being assembled to form the two-stage light gas gun.

(4) The diamond ablation study has been performed by injecting diamond pellets into the hot plasma of the Madison Spherical Torus (MST). It has been found that the diamond ablates at a rate significantly less than carbon pellets injected into the plasma for comparison.

The individual tasks associated with the TIP development are currently being completed. Integration of these tasks is currently underway. It is expected that the integrated system will be functional in the first six months of 1992.

Studies are currently underway to develop a sabot stripping system, and to develop a vacuum interface system between the TIP diagnostic and the plasma experiments' vacuum chamber.

1 INTRODUCTION

This report presents a summary of the work performed during Year 1 (9/15/90 - 10/15/91) for the Transient Internal Probe Diagnostic (TIP) experiment at the University of Washington, Seattle. This work has been performed under the Air Force Office of Scientific Research Grant #AFOSR-90-0345.

1.1 Research Objectives

The research objective of the Transient Internal Probe (TIP) program, presently under development in the Nuclear Engineering department at the University of Washington, is to permit the internal probing of the hot, high density plasmas currently used in magnetic fusion research. This is to be accomplished, first, by encasing the probe in a industrial diamond coating to reduce the boil-off, and second, by firing the probe through the plasma at high velocities to significantly reduce the amount of time during which the probe is in the plasma. Instead of using a probe that remains in the plasma for the lifetime of the plasma, the TIP concept fires the probe through the plasma on a much shorter time scale. The TIP concept can be extended to simultaneously measuring three components of the magnetic field, or by carrying onboard microelectronics, be extended to become a transient Langmuir, capacitive, pressure, or density probe. For the present proof-of-principle TIP development it has been proposed to measure only one component of the magnetic field (in the direction of the probe

trajectory) using a retroreflecting magneto-optic sensor and an external laser to relay the information from the plasma chamber. To complete this the following major tasks must be achieved: (1) The design and fabrication of a magneto-optic sensor integrated into a diamond projectile, (2) Development of an optical detection system capable of relaying the transient probes' measurements from the plasma chamber, and (3) Development of a light-gas gun capable of firing the transient probe to speeds in excess of 2 km/sec. A fourth task has also been recognized and added to the TIP development: A diamond ablation study to determine the interactive effects of the diamond projectile in contact with a hot, high density plasma.

1.2 Status

The initial stage of the TIP program has consisted of independent development of each of its main components. These are the two-stage light gas gun, the optical detection system, and the transient probe. As each of the individual components is brought to completion, the development of an integrated system is complicated by the need to meld the different vacuum, timing, and size requirements of each of the components, and determining the compromises that result in the best overall design for the TIP concept. Currently, in the TIP development, each of the individual components is either completed or near completion as detailed below. Further design studies are currently underway to determine the best timing and vacuum interfaces between TIP and a Tokamak fusion experiment.

1.2.1 Two-Stage Light Gas Gun

The design of the two-stage light gas gun has been completed by Mike Bonet, a graduate student under the supervision of Professor Walter Christiansen of the Aerospace and Astronautics department. The final design incorporates many improvements over the design shown in the previous progress report (3/15/91) and will be detailed in a later section. The gun is presently being fabricated. The main components, (the pump tube and gun barrel) are being constructed by off-campus contractors since they require machining beyond the capabilities of the University machine shops. Those components are expected to be completed and delivered in December, 1991. The remaining components, (driver tube, connecting flanges, inserts, etc.) are all being constructed in the Aerospace and Energetics Research Laboratory machine shop. Construction of these components is finished and integrating the components into the two-stage light gas gun is currently underway.

1.2.2 Optical Detection System

The final design of the optical detection system, which measures the angle of polarization of the retroreflected laser light, has been finalized and the construction of this optical detection system has been completed. The constructed system will be shown in a later section along with a method of using the optical measurements to calculate the internal magnetic field of a high temperature plasma. Presently the optical detection system is undergoing testing and calibration.

1.2.3 Probe Design and Fabrication

The probe fabrication can be divided into three essential goals. The first is to optimize the probe dimensions. The second is to determine a method of cutting the Faraday-rotator material into the optimal probe dimensions, and the third is to develop a means of polishing the cut probe to a high optical quality. The TIP concept is using Cadmium-Telluride that has been heavily doped (45%) with Manganese (CdMnTe) as its Faraday-rotator material because its high Verdet coefficient will result in a large change in the polarization angle of the retroreflected laser light. Due to the relative rarity of this material, little is known of the machining properties and polishing techniques.

The optimum design for the probe has been calculated using ray tracing programs that simulate incident laser beam and follow the reflected rays back to the detection system. This allows a calculation of the beam intensities at the detectors, which are maximized to find the correct probe length.

A method has been developed and tested for polishing CdMnTe to a high optical quality. The necessary diamond saw blades have been acquired and adapted to the equipment in the Material Sciences machine shop for cutting the Cadmium-Telluride. Measurements made of the index of refraction using the Cadmium-Telluride samples, show an index slightly higher than that used in the ray tracing programs. The effects of this increase on the probe dimensions are currently being investigated. Following this investigation, and a check of the optical detection system sensitivity, the probe will be fabricated.

1.2.4 Diamond Ablation Experiment

Diamond ablation studies have been performed to determine the effect of the hot plasma on the proposed diamond cladding for the TIP projectile. It is known that materials injected into a fusion experiment will suffer ablation as it comes into contact with the hot plasma. This method is often used as a method for fueling the plasma by injecting pellets of deuterium or, more recently, tritium. While the ablation rates for these materials are fairly well known, there is not an experimental data base for the ablation rates of diamond. To study these rates, small diamond pellets have been injected into the Madison Spherical Torus (MST) and the ablative effects have been measured. These measurements, detailed in a later section, show an ablation rate for the diamond pellets significantly less than that of carbon pellets that were injected for comparison purposes.

1.2.5 Personnel

The TIP research is led by Greg Spanjers, a researcher in Nuclear Engineering at the University of Washington. A graduate student in the Aerospace and Astronautics Department, Mike Bohnet, has been designing, constructing and testing the two-stage light gas gun as part of his Masters Degree under the guidance of Aerospace and Astronautics Professor Walter Christiansen. Professor Glen Wurden, of the Nuclear Engineering Department, has performed the diamond ablation studies. Professor Thomas Jarboe, of the Nuclear Engineering Department, lends overall guidance to the TIP development in his role as the Principle Investigator. Professor Jarboe is also the Principle Investigator for the Helicity Injected Torus (HIT) on which TIP will eventually be installed.

2 TWO-STAGE LIGHT GAS GUN

In this section the developmental status of the two-stage light gas gun, used to propel the TIP projectile, is reviewed. The current status is as follows:

1) The design of the gas gun has been finalized.

2) The construction of the individual gun components are either completed or will be completed within 30 days. The gun barrel and pump tube, being fabricated by outside sources, are expected for delivery within the month.

3) Possible sabot designs and stripping schemes have been investigated and design calculations are being performed on the two schemes that exhibit the most promise.

4) Issues associated with the vacuum and timing interface between the gas gun and the plasma experiment have been investigated.

The general configuration of a two stage light gas gun is shown in Figure 2.1. The two-stage light gas gun operates in the following manner: First, the piston is released by bursting a diaphragm, and the high pressure driver gas (2,500 psi) in the first stage accelerates the piston into the pump tube, subsequently pressurizing the propellant gas in the second stage to a pressure substantially higher than that in the first stage. As the second stage gas reaches the peak pressure (45,000 psi), a second diaphragm bursts, allowing the propellant gas to accelerate the sabot, (which holds the TIP projectile), down the barrel. This use of a

piston and pump tube greatly enhances the pressure and temperature of the propellant gas over what could have been attained by trying to preheat and pre-pressurize the propellant gas before firing.

It has been determined that the constant area two stage configuration, shown in Fig. 2.1a, has specific initial P1/P2 and L1/L2 ratios that together, will be associated with a minimum overall gun length L for a given initial driver pressure P1 and a desired probe velocity. A computer program, using the isentropic equations of a perfect gas to model the pump tube with a "slow" piston and quasi one-dimensional unsteady compressible flow (Riemann invariants) to model the expansion of the propellant gas as the sabot/tip package accelerates down the barrel, was initially set up for finding the minimum length of a two stage gas gun with constant area stages. The program has since then been modified to accommodate a gun with chambered stages. An example of a two stage light gas gun with chambered stages is shown in Fig. 2.1b. The important parameters for gun length minimization are now P1/P2 and V1/V2, which are the initial pressure ratio across the piston and the volume ratio of the two stages, and there will be specific P1/P2 and V1/V2 ratios that together will be associated with a minimum overall gun length for a given driver gas pressure P1, set area ratios A1/A2 and A2/A3, and desired probe velocity. A specific calculation using the above mentioned optimization scheme is given in Table 1 using Hydrogen as a propellant gas. The calculation in Table 1 uses pressures and dimensions that are roughly representative of the actual design choice, although some changes were made which will be discussed later in the report. In order to design the shortest possible gun, the area ratios should be made as large as possible. However, there are limitations to A2/A3, A1/A3 and A3/AS due to structural and fluid mechanical considerations. The larger these area ratios are, the larger the tube diameters must be in comparison to the sabot diameter. This increases the stresses in the material for a given maximum design pressure, consequently making the tubes more costly and difficult to manufacture. The ratio A2/A3 is more severely limited because the pressure is highest in that portion of the gun and a larger A2/A3 means increased difficulty, from a fluid mechanical standpoint, in forcing the propellant gas to transition from A2 to A3. However, with the area ratios that were chosen (stated in Table 1), the overall length of the gun has been significantly reduced below what it would have been had a constant area light gas gun been chosen.

The gun design was essentially finalized using the above mentioned computer program, except for a modification which will now be discussed. An actual drawing of the two stage light gas gun being fabricated is shown, to scale, in Fig. 2.2. The modification is the perpendicular

Table 1: Predicted Performance Characteristics of Two-Stage Light Gas Gun

Initial Conditions	
$Probe\,Velocity = 2000\frac{m}{s}$ $\frac{A_1}{A_3} = 23.7$ $\frac{A_2}{A_3} = 6.35$ $sabot: \frac{mass}{area} = 1.50 gm/cm^2$	$P_1 = 2500\,p.s.i.$ $T_1 = 300\,K$ $\frac{A_3}{A_s} = 3.00$ $piston: \frac{mass}{area} = 27.0 gm/cm^2$
Ratios for Minimum Gun Lengths	
$\frac{V_1}{V_2} = 1.87$	$\frac{P_1}{P_2} = 13$
Results	
$P_3 = 45,600\,p.s.i.$ $L_3 = 0.26m$ $L_2 = 1.96m$ $\text{Max. } Piston\,Velocity = 227\,m/s$	$T_3 = 1430\,K$ $L_2 = 0.37\,m$ $L_1 = 1.00m$ $L = 2.59\,m$

orientation of the reservoir for the driver gas which will be referred to as the driver tube. The benefit from the perpendicular arrangement of the driver tube is twofold: First, the overall length of the gun is reduced, and second, the geometry of the perpendicular arrangement allows the use of a more convenient and reliable piston release mechanism. Two stage gas guns with a gas driver normally use either a single diaphragm or a double diaphragm method of piston release. Both of these methods rely on the bursting of disposable diaphragms to initiate piston motion. This means the diaphragms must be replaced after each shot; a method that is not very time effective because a gun joint must be constantly opened and closed. Diaphragms that are designed to burst at a certain pressure also exhibit an amount of uncertainty in the actual value of their burst pressure and sometimes, instead of immediate rupture, the diaphragm will "hang" for a time before rupturing or it will relieve itself by letting the pressure leak slowly through a crack in one of the scorings. Either one of these scenarios is unacceptable.

A less cumbersome and time consuming method of piston release has been found, as shown in Fig. 2.2. Before each shot the entire gun is pumped down to clear it of heavier gases (i.e. Oxygen). However, the barrel may be pumped down to a relatively hard vacuum in order to be compatible with the plasma device. The pump tube is then filled with the propellant gas to the required pressure P2, followed by the filling of the driver tube with the driver gas to the required pressure P1. The piston is now being pushed backwards against the piston stop, which has been opened to the atmosphere, by the propellant gas. The piston is also blocking the two holes that allow the driver gas to flow into the pump tube. When firing is desired, the piston stop is closed to the atmosphere and connected via plumbing (not shown) to the driver tube which now pressurizes the back side of the piston, pushing it forward, thus uncovering the holes allowing the driver gas to be dumped into the pump tube. This pushes the piston down the pump tube which compresses the propellant gas causing the gun to fire.

The materials for the gun components were chosen for high strength and ease of manufacture. The pump tube and the barrel are made from 4340 alloy steel because, in the hardened and tempered condition, 4340 exhibits a good combination of high yield strength and ductility. Making these parts out of alloy steel is also less time consuming and less expensive than building a composite or pre-stressed tube. The perpendicular driver tube is made out of 1018 carbon steel. Carbon steel was chosen over alloy steel for this application because of the need for a welded joint as shown in Fig. 2.2. Alloy steel could be welded but the cost would have been higher and a post-weld heat treat would have been required to

lessen the effects of the heat affected zone around the weld. Presently, the perpendicular driver tube has been welded by a certified welder and has been checked for cracks and found to be acceptable.

The major gun sections, the driver tube, the pump tube and the barrel, are joined together with bolted flange connections. To minimize cost, the flanges for the bolted connections are not machined from the same stock as the tube, rather they are designed to be screwed on to the ends of the tubes. Both the tubes and the flanges are slightly over-designed with high safety factors, not only for stress reduction, but also for minimum elastic displacement under loads, which insures the proper performance of the O-ring face seals. The bolted connections are also designed such that a significant compressive load still exists on the joint when maximum pressure occurs in the tube. The maximum allowable operating pressures for the different gun sections along with their appropriate bolted flange connections are:

Driver Tube:	4,200 psi
Pump Tube:	50,000 psi
Barrel:	50,000 psi

These components will be hydrostatically pressure tested upon their arrival from the manufacturer.

A critical part of the gun which strongly affects its performance is the diaphragm between the propellant gas and the sabot/TIP package. This diaphragm will also suffer from the same inherent uncertainty in burst pressure mentioned above. If this diaphragm bursts at a lower pressure than desired, the TIP's final velocity will be reduced. If the diaphragm does not burst or bursts on the second or third piston stroke, the gun will fire unpredictably or it will not fire at all. Therefore, it is important that the diaphragm be properly designed and to this end a good report by the U.S. Naval Ordinance Laboratory on the design of flat-scored high pressure diaphragms was recommended by other light gas gun experts, and has proven to be extremely helpful in the design of a suitable diaphragm for our gun. Fortunately the burst reliability of this diaphragm, unlike the diaphragms used for initiating the piston motion, is assisted by the rapidly increasing pressure in the pump tube, making the prospect of using a diaphragm for sabot launch more appealing. Fine tuning of the diaphragm will be accomplished through a program of laboratory testing.

In addition to just a two stage light gas gun for accelerating the sabot/TIP package, a method must be devised to strip the sabot allowing only the TIP projectile to travel through the plasma device. A vacuum interface must also be constructed to preserve the hard vacuum in the plasma device and also to prevent the propellant gases from entering the experiment and quenching the plasma.

A number of sabot stripping techniques have been investigated and two of them stand out to be the most promising for our application. The first and the easiest to build is the axially separating sabot stripper which is shown in Fig. 2.3. The sabot for this scheme would be a single piece sabot made out of lexan or some other high strength plastic. When the sabot reaches the end of the barrel it encounters the sabot stripper which has a discontinuity or a step in diameter. Upon contact with the step the sabot will encounter a decrease in acceleration while the TIP projectile, which is free to slide forward in the axial direction, will encounter relatively little decrease in acceleration. The TIP projectile will then pass through an even smaller hole that will be too small for the sabot to pass through, thus, effectively stripping the sabot from the TIP projectile. The TIP projectile then passes through the vacuum interface shown in Fig. 2.4, to the plasma machine. This vacuum interface consists of a large vacuum tank with baffles installed to inhibit any gas, that might leak around the sabot, from getting into the experiment before the gate valve can be closed. The sabot stripper is connected to the vacuum tank with a sliding O-ring seal which enables the gun to slide with respect to the vacuum tank. In this way the recoil of the gun will not be transferred through the tank to the plasma device. With this first sabot stripping scheme, the barrel need not be rifled or vented, and the sabot has a very simple design which makes this scheme very easy to build.

The second sabot stripping technique that will be considered entails the use of a rifled and vented barrel and the sabot must have a more complicated design. This technique is called the radially (spin) separated sabot stripper and it is shown in Fig. 2.5. The sabot for this scheme is made up of an obturator, the piece that seals the sabot, preventing the gas from leaking around the sabot, and two to four petals that support the projectile during it's ride down the barrel and later radially separate from the projectile after the muzzle of the barrel is cleared. Spin is acquired by the sabot/TIP package through the rifling in the barrel, so when the sabot/TIP package exits the barrel the petals travel away from the TIP projectile trajectory due to centrifugal effects. The TIP projectile then travels through a hole in plate that is made from a material that is easily cratered, while the petals impact with the plate adjacent to the hole. The craters that result would swage the hole shut, and the obturator would then impact the closed plate, thus leaving the TIP projectile alone to travel through the experiment. Gas

expansion slots are cut into the gun barrel just before the barrel to relieve any excess gas pressure before the projectile exits the barrel. If slots were not cut there, the gas immediately behind the sabot, which is energetic enough to accelerate rapidly once the sabot leaves the confines of the barrel, would shoot past the sabot/TIP package causing a reverse flow region to develop. This reverse flow region would interfere severely with the normal separation of the sabot petals causing failure of the petals to swage shut the hole in the plate, or possibly causing a petal to follow the TIP projectile through the hole. This, of course, would not be desirable.

The vacuum interface for this second sabot stripping scheme is shown in Fig. 2.6. One of the vacuum tanks is used this time as a dump tank to receive the gas from the expansion slots in the barrel, and the other contains baffles that would delay the gas from entering the experiment in the event that some gas escaped through the hole before it was swaged shut. The sabot stripper in this case is also connected to the vacuum tank through sliding O-ring seals again for the purpose of preventing the recoil of the gun from being transferred to the plasma device. This radial sabot stripping technique, unlike the first, has been tried before and made to work with outstanding reliability, although it is more complicated and harder to manufacture. It is our plan to implement the axial technique first and, if unsuccessful, the radial technique would then be used.

The course of action to be taken, that will lead to the eventual firing of the gas gun, is as follows. The different components of the gas gun will be tested separately in a progressive pattern such that after each testing phase another component will be added to the system and then the larger system will, in turn, be tested. Thus the testing of the system with the last component added will, in essence, be the first firing of the gun. A rough overview of the testing order is as follows:

1) Hydrostatic testing of the driver tube to 5000 psi.
2) Joining of the pump tube to the driver tube and testing the piston rings for leakage.
3) Testing the workings of the piston valve insert/piston and it's ability to hold gas in the driver tube for an extended period of time.
4) Progressive testing of the pump tube and it's ability to pressurize thepropellant gas by gradually increasing the ratio P1/P25).
5) Testing the burst pressure of the diaphragm.
6) Joining the barrel and vacuum tank to the rest of the gun and testing the speed of the sabot/TIP package.

7) Testing the axial sabot stripping technique and verification of the TIP projectile orientation and condition with high speed photography.
8) Testing of the radial sabot stripping technique and verification of the TIP projectile orientation and condition with high speed photography (if needed).
9) Joining the gun system to a plasma device and appropriate catch tube and optics for test measurements of one component of the internal magnetic field.

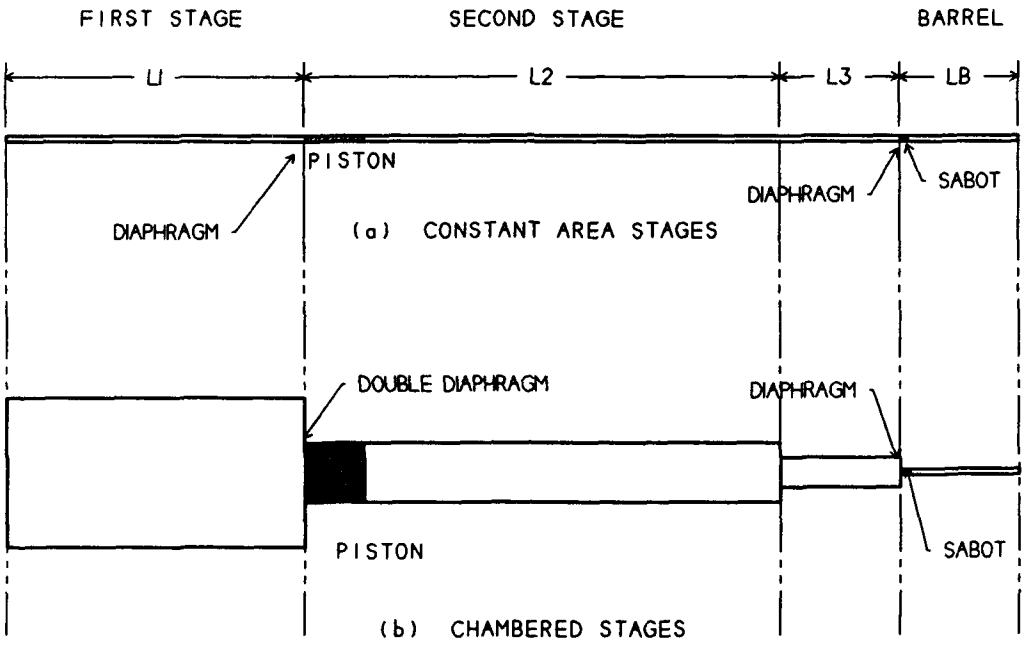

Fig. 2.1 Configuration of a two-stage light gas gun

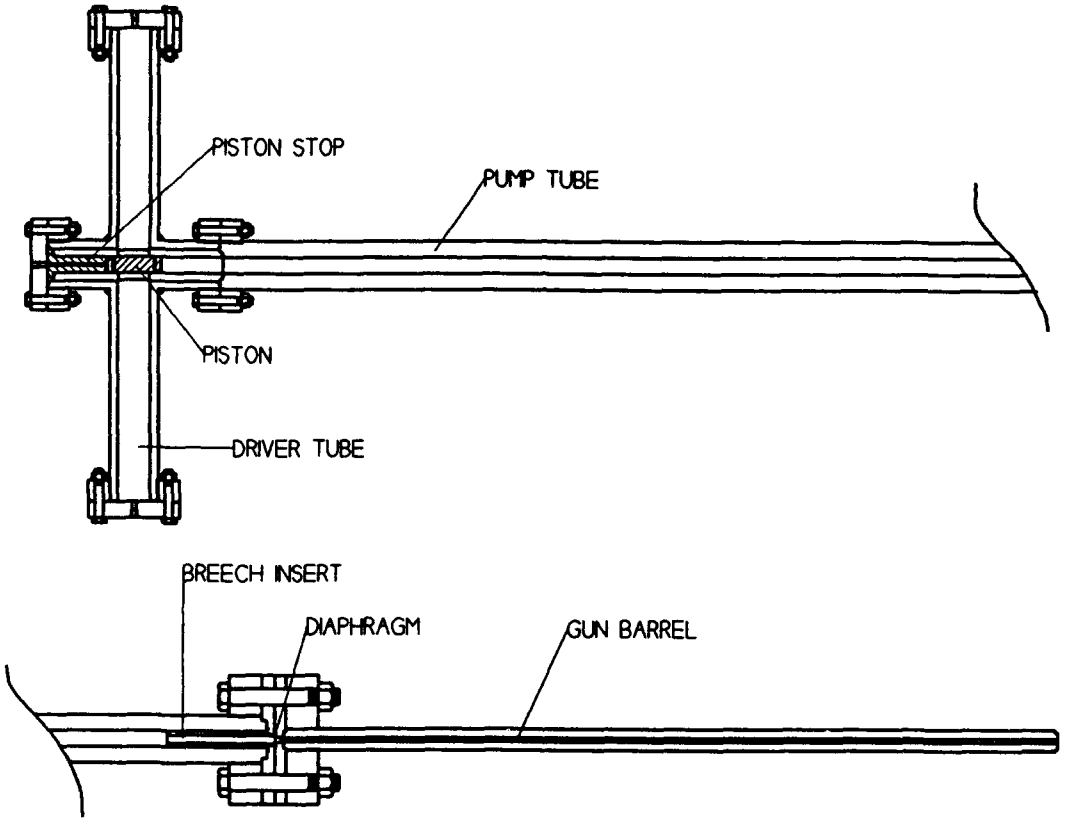

Fig. 2.2 Two-stage light gas gun being fabricated for the TIP program.

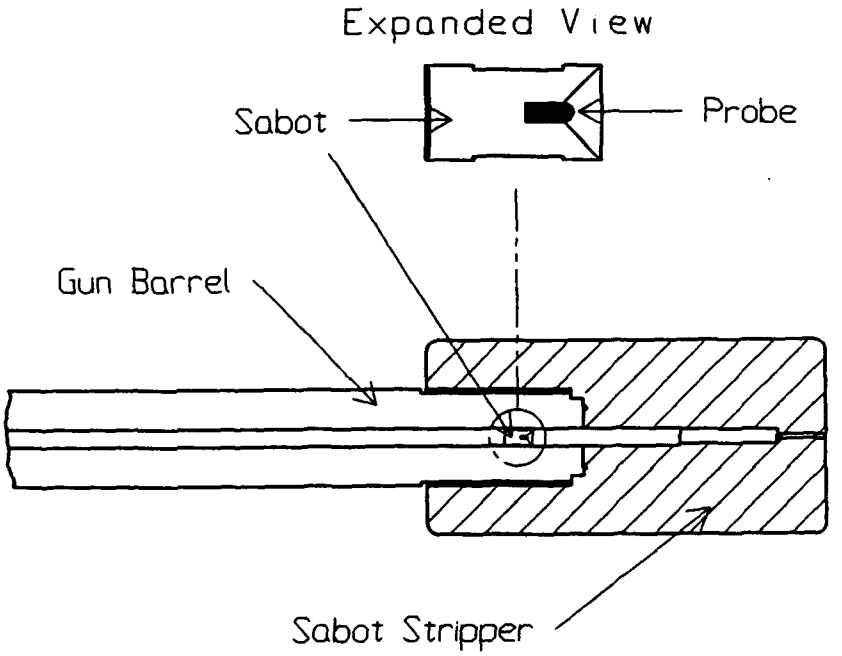

Fig. 2.3 Axially separating sabot stripper

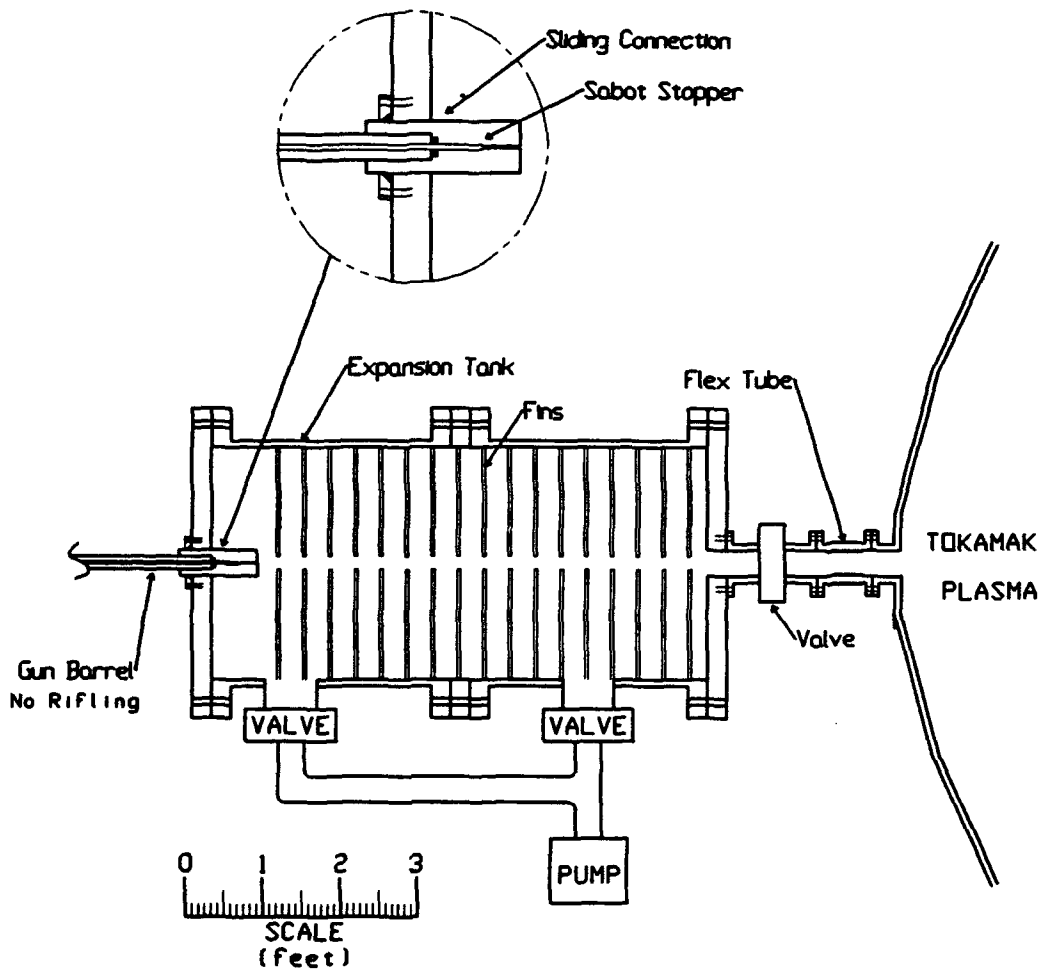

Fig. 2.4 Vacuum interface for the axially separating sabot stripping scheme

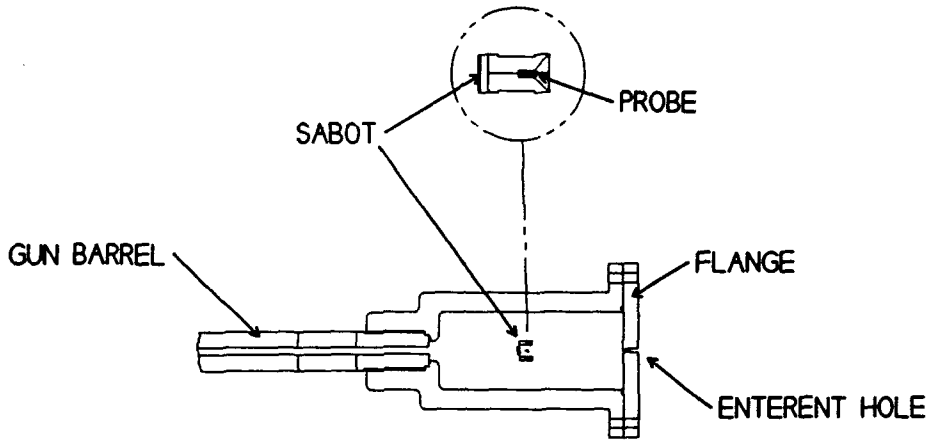

Sabot leaves gun barrel and begins to separate

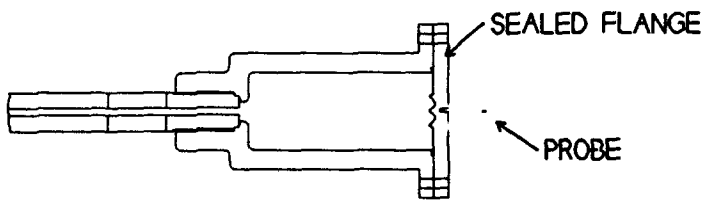

Probe passes through flange and separated sabot swages it shut

Fig. 2.5 Spin separated sabot stripper

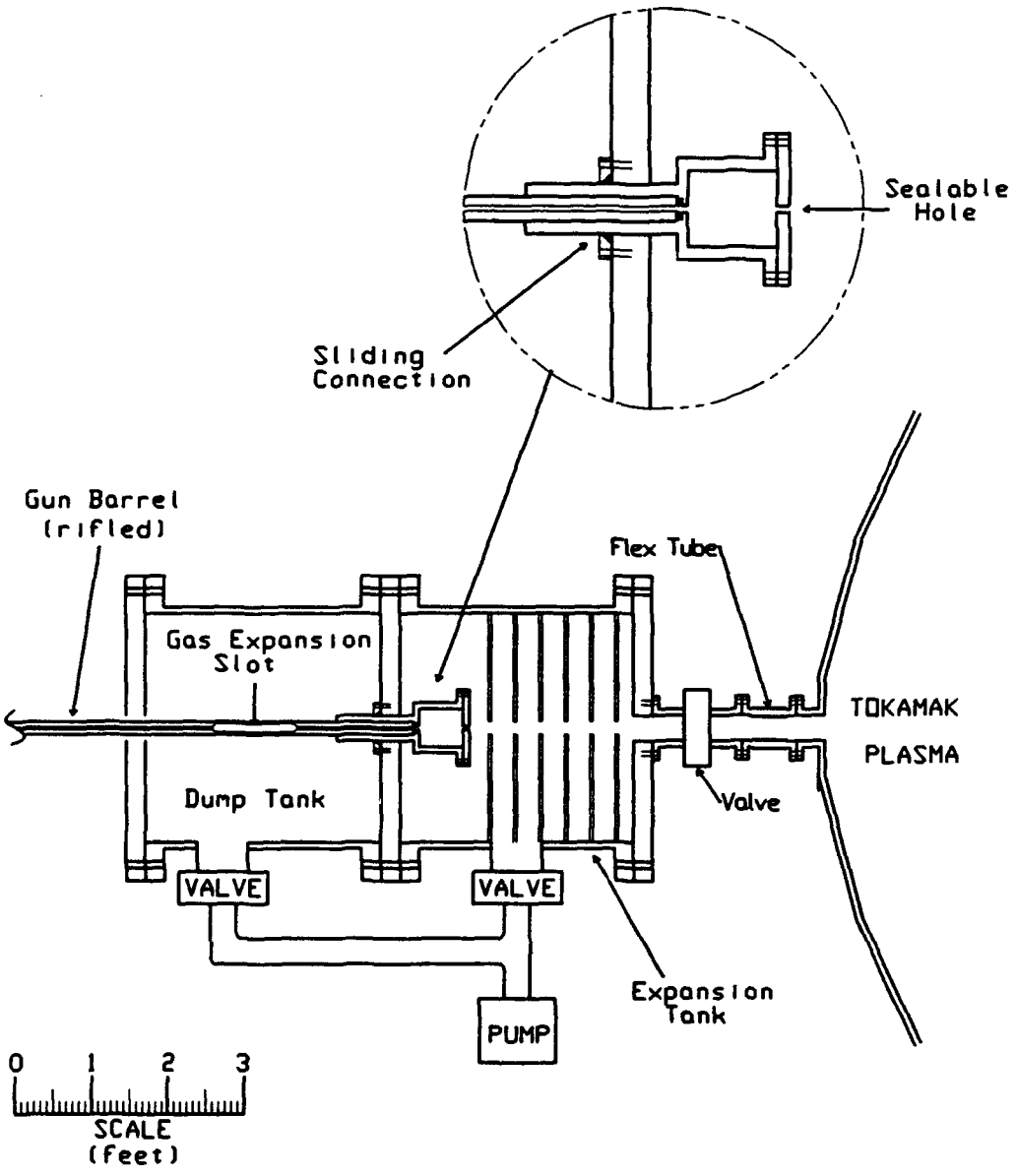

Fig. 2.6 Vacuum interface for the spin separating sabot stripping scheme.

3 OPTICAL DETECTION SYSTEM

Significant progress has been made towards the production of the optical detection system. The majority of effort has been directed toward the production of components to support the optical detection system. Final assembly of the system is complete. Testing, and calibration of the system is currently being performed.

3.1 Detection Scheme

3.1.1 Theory of measurement

The purpose of the electrical detection system is to measure the polarization angle rotation, due to the Faraday effect, by measuring the change in intensity of the incident light on the detectors. This requires developing a relationship between the polarization angle, Ψ, and the amplitude of the wave. Nominally this is

$$|E|_{rotate} = E_o \cos\Psi$$

Converting this to power

$$P = E_o^2 \cos^2 \Psi$$

Ideally this could be determined directly by comparing the reduction in signal to a signal from a known polarization angle. However, other factors affect the amplitude of the incoming signal, specifically, wave attenuation and background light sources. Taking these factors in to account with a scaling factor, C, and offset Σ, the power equation then becomes

$$P = C \cos^2 \Psi + \Sigma$$

Having three unknowns requires three equations to be solved simultaneously for the variables Ψ, C, and Σ. Three detectors, with polarizing filters at different angles, provide the necessary three equations:

$$P_o = C \cos^2(\Psi - \alpha_o) + \Sigma$$
$$P_1 = C \cos^2(\Psi - \alpha_1) + \Sigma$$
$$P_2 = \cos^2(\Psi - \alpha_2) + \Sigma$$

If the three polarizing filters are set at equal angles of $\alpha = 60°$, the equations become:

$$P_o = C \cos^2 \Psi + \Sigma = \frac{C}{2}(\cos 2\Psi + 1) + \Sigma$$

$$P_1 = C \cos^2\left(\Psi - \frac{\pi}{3}\right) + \Sigma = \frac{C}{2}\left(-\frac{1}{2}\cos 2\Psi + \frac{\sqrt{3}}{2}\sin 2\Psi + 1\right) + \Sigma$$

$$P_2 = C \cos^2\left(\Psi - \frac{2\pi}{3}\right) + \Sigma = \frac{C}{2}\left(-\frac{1}{2}\cos 2\Psi - \frac{\sqrt{3}}{2}\sin 2\Psi + 1\right) + \Sigma$$

These equations are solved using a least-squares minimization of the quantity R, where R is given by

$$R = \left\{\frac{C}{2}(\cos 2\Psi + 1) + \Sigma - P_o\right\}^2 + \left\{\frac{C}{2}\left(-\frac{1}{2}\cos 2\Psi + \frac{\sqrt{3}}{2}\sin 2\Psi + 1\right) + \Sigma - P_1\right\}^2 + \left\{\frac{C}{2}\left(-\frac{1}{2}\cos 2\Psi - \frac{\sqrt{3}}{2}\sin 2\Psi + 1\right) + \Sigma - P_2\right\}^2$$

The R minimization, $(dR/d\Psi = 0)$, results in an expression for the polarization angle Ψ:

$$\tan 2\Psi = \left\{ \frac{\sqrt{3}(P_1 - P_o)}{2P_o - P_1 - P_2} \right\}$$

This result for Ψ is valid only at equal $\alpha = 60°$ angles.

3.1.2 Calibration and Polarization Angle Calculation

In general, the detector polarizing filters will not be at equal $\alpha = 60°$ angles. To more accurately measure the angle of polarization, this can be accounted for in the calculations by considering the case of arbitrary angles, where the solution is found from a converging iterative analysis from the ideal case where $\alpha = 60°$ equal angles.

For arbitrary angles, the offset and scaling terms do not simply cancel. To solve this using an iterating method the system must be calibrated. The individual detector power equations are written as

$$S_i = A_i I_o + b_i P \cos^2(\Psi - \alpha_i)$$

where $A_i I_o$ represents the offset due to background unpolarized light, and $b_i P$ represents the scaling factor. An unpolarized light source, I_o is applied to the detectors. Solving for A_i:

$$A_i = \frac{S_i}{I_i}$$

A_i is then normalized such that $\sum_i A_i = 3$. A known source of polarized light is then applied to the detectors. By varying the polarization angle, b_i and α_i can be determined by solving simultaneous equations involving only b_i and α_i.

Once calibrated, the problem is solved for arbitrary angles using an iterating method and the least squares approach. The values for the coefficients are written as equations of summations. Assuming the initial condition of α_i being $60°$ apart, an initial value of Ψ can be obtained using only the measured values S_i as was previously shown. Taking this value of Ψ

and substituting into the equations for I and P, a new value of Ψ is obtained. This is iterated until $\Delta\Psi$ between iterations is acceptably small. The magnitude of the magnetic field B is then determined by

$$B = 2LV(\Psi - \Psi_o)$$

where L is the length of the Verdet material, V is the Verdet coefficient for the Faraday probe material, $\Psi - \Psi_o$ represents the change in the angle of the incident polarized light after reflecting through the probe.

Error analysis calculations have been performed for the polarization angle measurement. $\delta\Psi$ is found to be proportional to $\frac{\delta P}{P_{total}}$. Consequently, δB is independent of the magnetic field measurement B, leaving the accuracy of the measurement to be determined by the limiting accuracy of the data acquisition system used. For example, if the data were to be stored in an 8-bit digitizer with 256 count range, the error in the measurement would be

$$\frac{\pm 1\,count}{256\,counts} \approx 1\%$$

3.1.3 Description of Optical Detection System

The physical layout of the optical detection system consists of two levels. The lower level, shown in Fig. 3.1a, provides the illuminating light source for the system. The light source is a He-Ne laser with a 632nm wavelength. The laser beam passes through a 5 mm dia. and a 25 mm dia. lens spaced to act as a beam expander. A mirror at a $40°$ angle then reflects the light into the upper level of the system.

The upper level, shown in Fig. 3.2b, consists of a beam splitter, a combined lens and filter, two more beam splitters, three polarizing filters, and the detectors. As the beam impinges on the beam splitter, it is directed out towards the probe where it is retroreflected back to the optical detection system. The beam then passes though a focusing lens and filter. The filter is a band pass filter with peak transmission passing the 632 nm light from the He-Ne laser and band with of ±10 nm. The beam continues passing through the remaining beam splitters to be

directed to the individual polarizing filters and detectors. These polarizing filters establish the angles, α_i, previously discussed. The spacings between optical components have been chosen such that incident angles on optical components and overall size remain small to minimize measurement errors. Dimensions for the total optical detection system, including a protective beam dump enclosure (not shown in the figures), are 75 cm long, 25 cm high, and 30 cm wide.

The system support components have been designed to allow position adjustment in every plane of motion while minimizing the overall size of the optical detection system. The desire to minimize size was based on reducing the impacts of the detection system in the space surrounding the plasma machine. The resulting design height which accommodated each component is 7.5 cm from the surface to the center line of the beam. All components on the lower level are mounted on a single track with carriages designed to allow motion along the direction of the beam only. All components on the upper level are mounted on a similar track also, with the exception of the two angled detectors. These are mounted on separate tracks with their respective filters. Once aligned, the entire detector system will be enclosed in a removable cover to minimize background light.

The design of the three photodetector assemblies is shown in Fig. 3.2a. They have been engineered to allow the polarizing filter to be rotated as required for initial calibration while maintaining the focal point of the lens precisely on the surface of the photo diode. The filter and lens assembly consists of the focusing lens which is directly mounted to the polarizing filter using an optical cement with an index of refraction nearly matched to that of the lens. These components are then housed in an outer canning which rides in a groove on the main detector housing and can be rotated as required for system calibration. The detector housing holds the filter lens assembly and is threaded to allow the photo diode assembly to be positioned relative to the focal length of the focusing lens. The photo diode assembly consists of nylon hollowed out on the inside to hold the photo diode and threaded on the outside to position the diode. An insert to secure the diode and a mounting pad with counter weights for balancing is attached to allow the detector to be mounted on the system tracks.

The completed optical detection system, with the beam dump and cover removed, is shown in Fig. 3.2b. Currently the system is being tested and calibrated, which will be completed shortly.

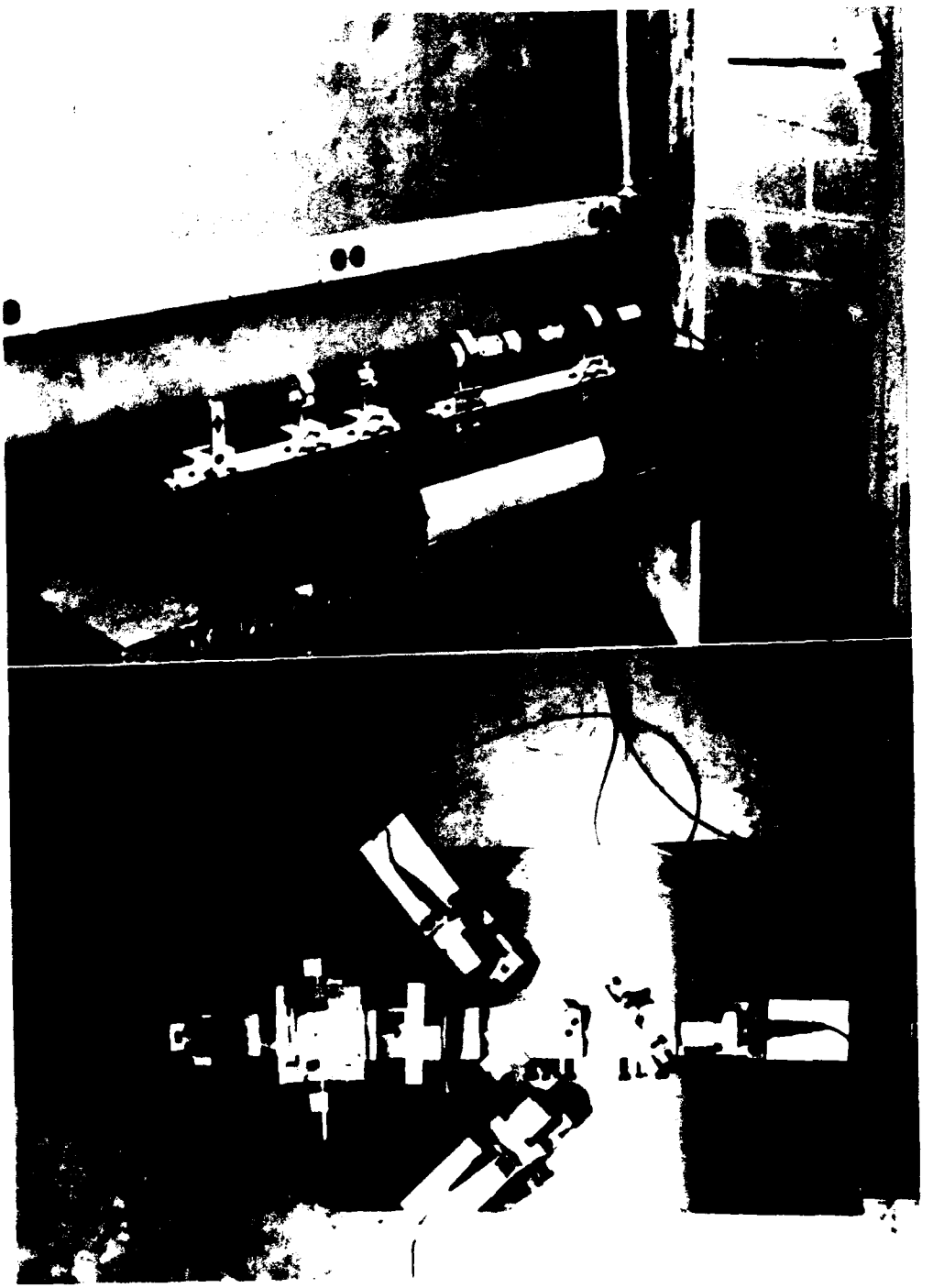

Fig. 3.1 (a) Side view of lower level (upper level removed) of optical detection system showing the laser and beam expander, and (b) top view of upper level showing the layout of the photodetector housings and beam splitters.

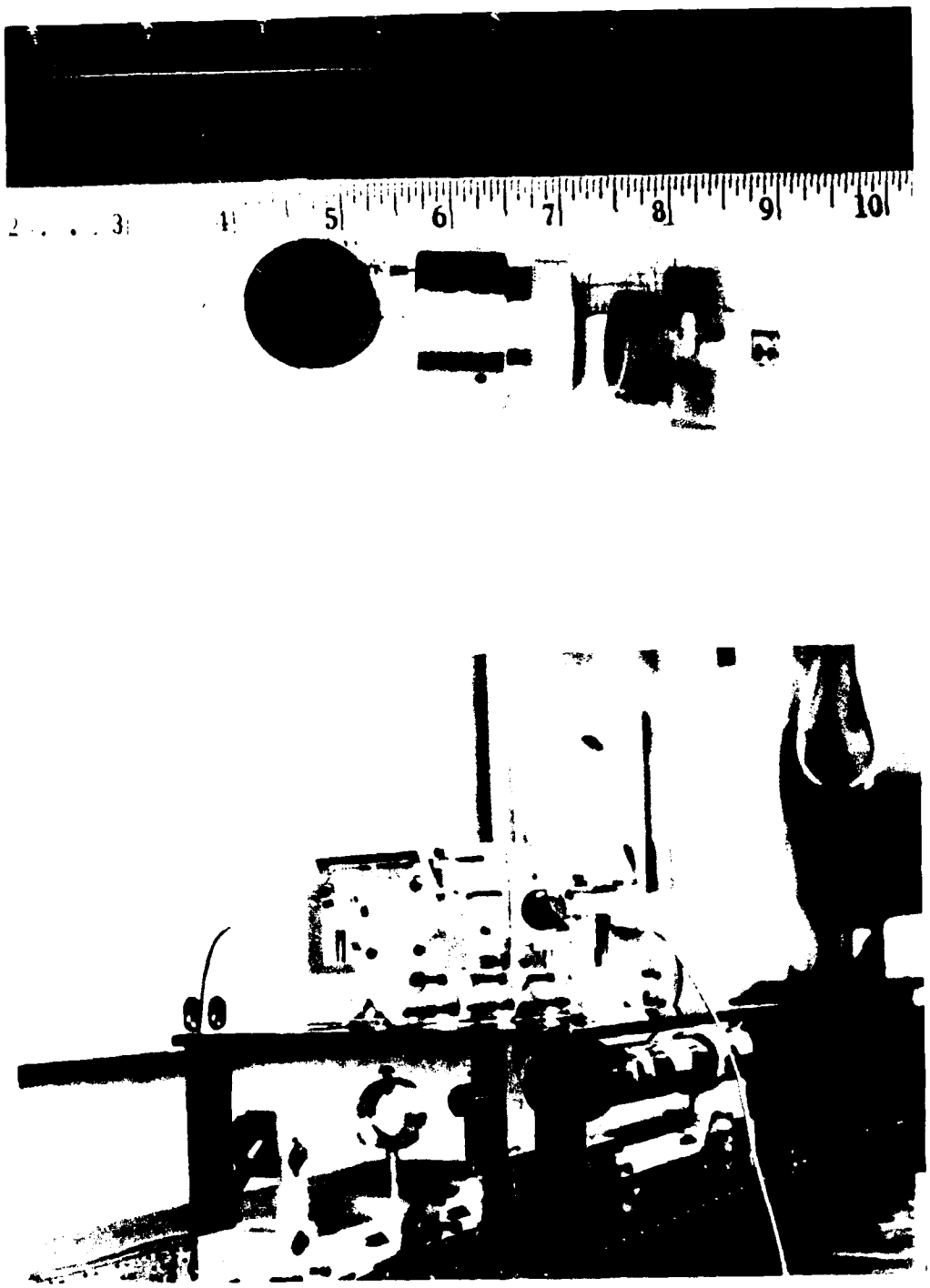

Fig. 3.2 (a) Assembly of photodetector housing showing the lens, polarizing filter, housing, and photodiode, and (b) Full layout of the optical detection system. The beam dump and cover have been removed to show the individual components.

4 PROBE DESIGN AND FABRICATION

The probe design for the TIP concept consists of a Faraday rotator material encased in a diamond cladding, as shown in Fig. 4.1. An external polarized light source incident on the probe, suffers a change in polarization proportional to the local magnetic field, and is retroreflected to an optical detection system where the change in polarization is measured. The local magnetic field, at the position of the probe, can then be calculated as

$$B_{||} = \frac{\Delta\theta}{2VL}$$

where $B_{||}$ is the local magnetic field in the direction of the laser beam in the probe, $\Delta\theta$ is the change of the polarization angle of the incident laser beam, V is the Verdet coefficient of the probe material (≈0.17 deg/Gauss/cm. for Cadmium Telluride with the Manganese doping, and L is the length of the probe.

4.1 Probe Design

For the optimal probe design, we wish to maximize the retroreflected laser light that enters the optical detection system by varying the probe dimensions. This optimization procedure has been performed using ray tracing codes that simulate the incident laser beam rays, and follow the progress of each beam through the reflections and transmissions at each interface.

Studies with the ray tracing programs have found that a 2mm diameter microlens with a 1.57 mm focal length attached to a 3.913 mm probe gives the optimal reflected power to the optical detection system. For the high index of refraction of the Verdet material (n=2.6), the lens-probe combination has an effective focal length of 4.08 mm.

The reflected intensity is maximized by fabricating the probe slightly shorter than the optical focal length. This optimal probe length is illustrated in Fig. 4.2 which shows the beam divergence (in terms of the angular deflection) for various probe lengths, as calculated by the ray tracing programs. In Fig. 4.2a the fraction of rays within a given divergence is plotted versus the divergence angle for various probe lengths. The graph shows that for the shortest probe lengths, the fractional angular distribution is hollow, indicated by the relatively low fractions at small angles and a sharp increase at some larger critical angle. The hollow profile is undesirable since the larger deflection angles necessary to focus the rays in the optical detection system increases the error in the polarization measurement. For the longest probe lengths the profile is no longer hollow, however the asymptotic intensity at large angles begins to decrease indicating that a fraction of the rays incident on the probe do not reflect back to the optical detection system. This is undesirable since it is desirable to maximize the reflected laser intensity at the detectors. These two effects are better illustrated in Fig. 4.2b where the fractional angular distribution is plotted versus probe length for several reflection angles. Figure 4.2b shows that for small angular distributions, the fraction of rays within the angle peaks between the 3.9mm and 3.98 mm probe lengths.

The effects of a probe wobble have also been considered. Calculations have shown that, if probe wobble occurs, the magnitude will be small. (The magnitude of any probe wobble can be lessened by minimizing the distance from the gun barrel to the experimental chamber thus affecting the design of the vacuum system interface.) The effects of a 6° probe wobble are shown in Fig. 4.3 which are identical to the calculations leading to Fig. 4.2 with the angular deviation of the probe added into the analysis. Comparing the graphs of Figs. 4.2 and 4.3 shows that as the probe tilt increases, a shorter probe becomes more effective in maximizing the power intensity at the detectors.

Subsequent measurements made of the index of refraction for our CdMnTe sample have shown that it has a value of $2.8 \pm .1$, whereas the ray tracing analysis used an index of 2.6. This will result in a slightly longer probe than that found to be best using the ray tracing analysis.

4.1.1 Probe Fabrication

The major concern of probe fabrication is to develop a methodology whereby the CdMnTe Faraday material can be cut within the stringent geometric constraints and then polished to an optical quality. Due to CdMnTe being a state-of-the-art material, little is known about either its machining properties or its optimal polishing technique. Previous research, at Sandia, using this material did not have the stringent tolerances that we have in the TIP development. At Sandia they were able to simply cleave the material and then polish it using a Bromine-Methanol solution. This method is unacceptable for TIP purposes for two reason. First, cleaving will not allow probe fabrication to an accurate length, and second, the low etch rate of the Bromine-Methanol solution will not significantly alter the length of the probe. A rough grinding technique in needed that will allow the fine tuning of the length for proper focusing of the bilith lens-probe combination. Additionally, the Bromine-Methanol solution is extremely toxic and is preferably avoided if a better method can be found.

The method developed for cutting and polishing the CdMnTe is as follows:

1. Rough cut using diamond saw blade.
2. Sand faces smooth with 600 grit Silicon Carbide paper.
3. Sand faces with 800 grit Silicon Carbide paper - wash with distilled water.
4. Polish faces using 6 micron diamond abrasive on optical mat.
5. Lubricate with small amounts of oil and repeat (4) - wash.
6. Polish with Silica Suspension fluid on same optical mat - wash.
7. Polish with same Silica Suspension fluid on optical polishing microcloth - wash.

This method has been tested and found to give a good optical finish. Fine adjustments to the probe length can be made using the 600 grit Silicon Carbide paper and repolishing. Once the probe is polished, arrangements have been made to have the rear reflector end aluminized in the Material Science machine shop.

The total probe fabrication will take only a few hours. The actual fabrication will be performed once the optimal probe length is certain. The final probe length calculation depend only on the sensitivity of the optical detection system, which will be tested shortly, to determine the allowable reflected beam deflection and intensity.

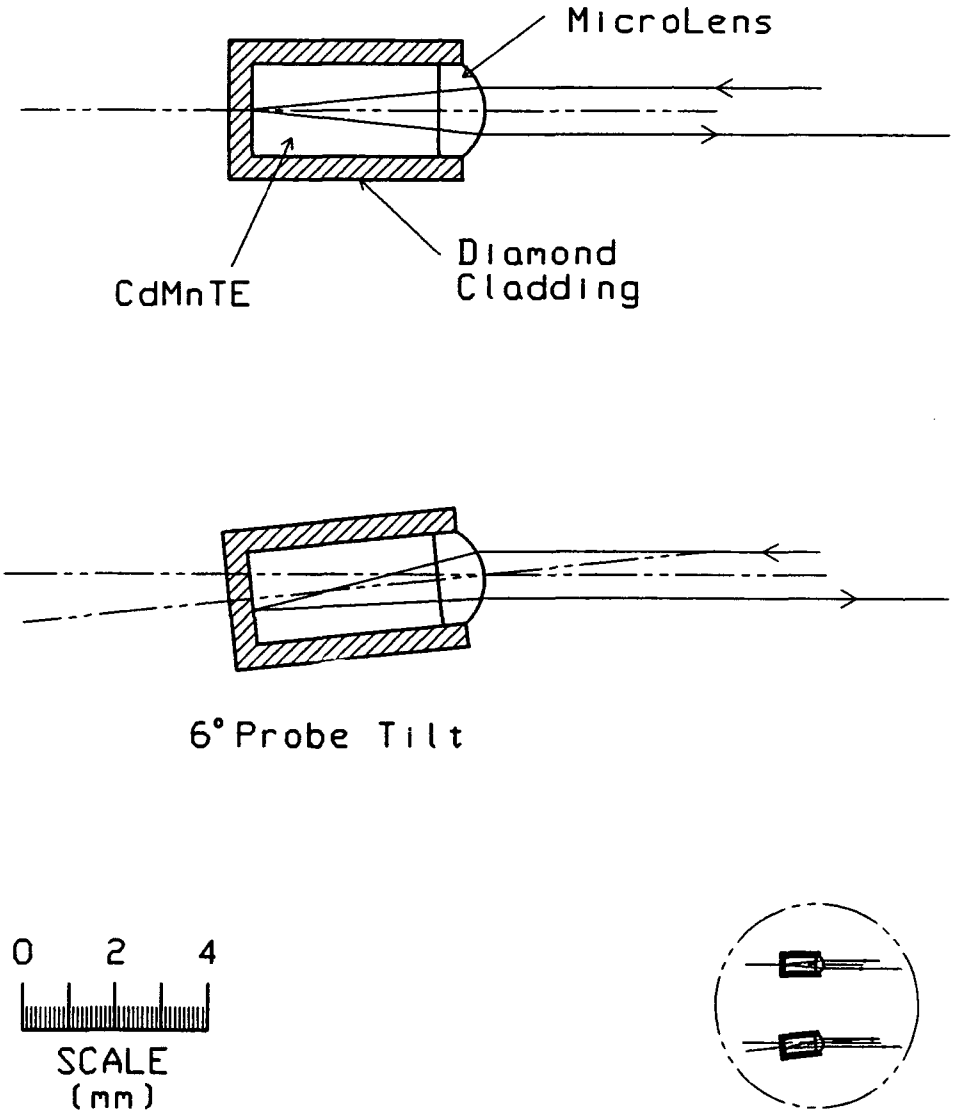

Fig. 4.1 Diagram of TIP projectile with the Verdet material encased in a diamond cladding with a small microlens attached. The lower diagram shows the probe with a 6° tilt due to probe wobble as investigated with the ray-tracing analysis. For size comparison, the inset in the lower right corner shows the projectile with its true size (scale=1).

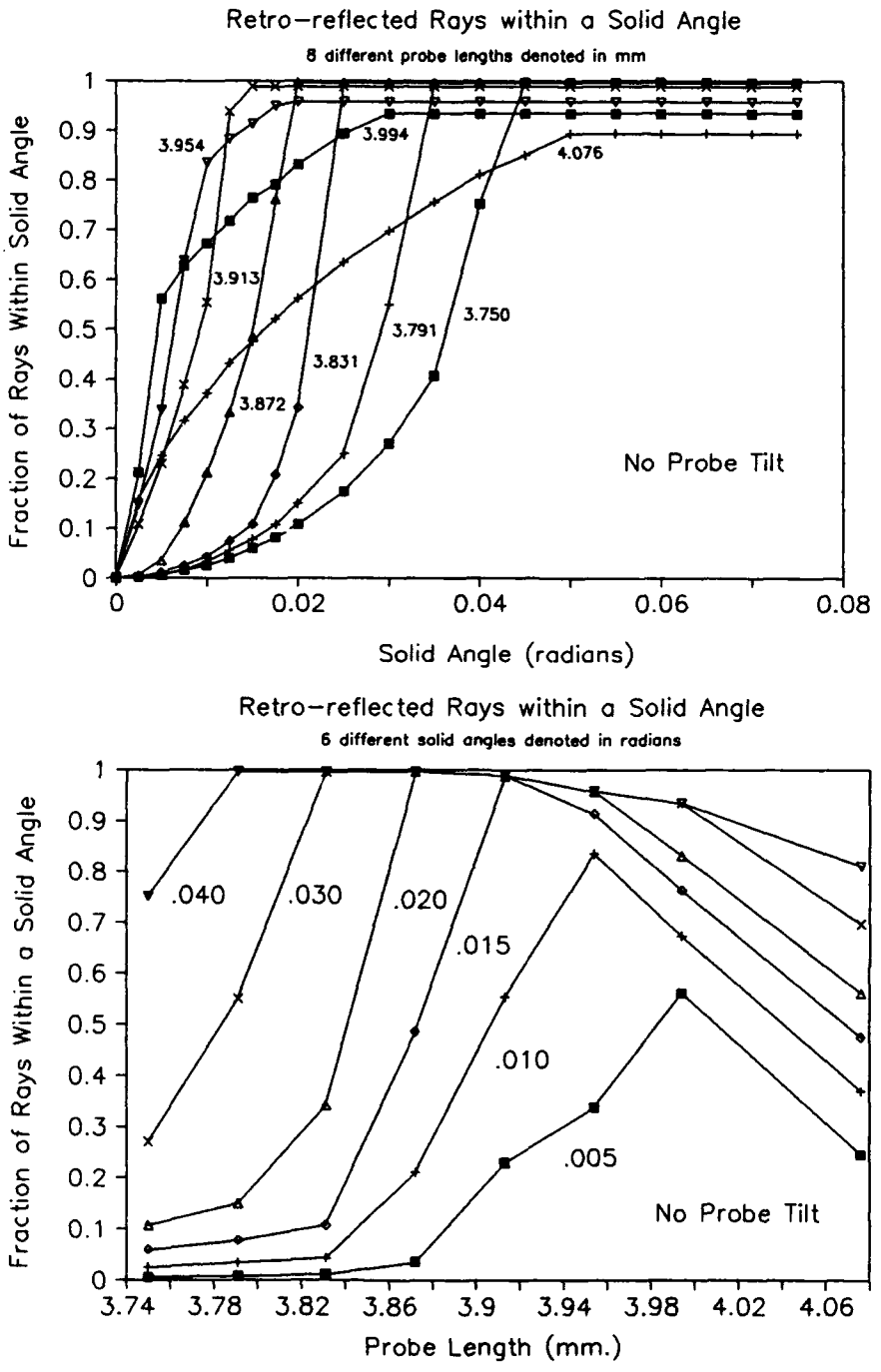

Fig. 4.2 Retroreflected beam divergence calculated for the TIP projectile using ray tracing programs for the case of no probe tilt.

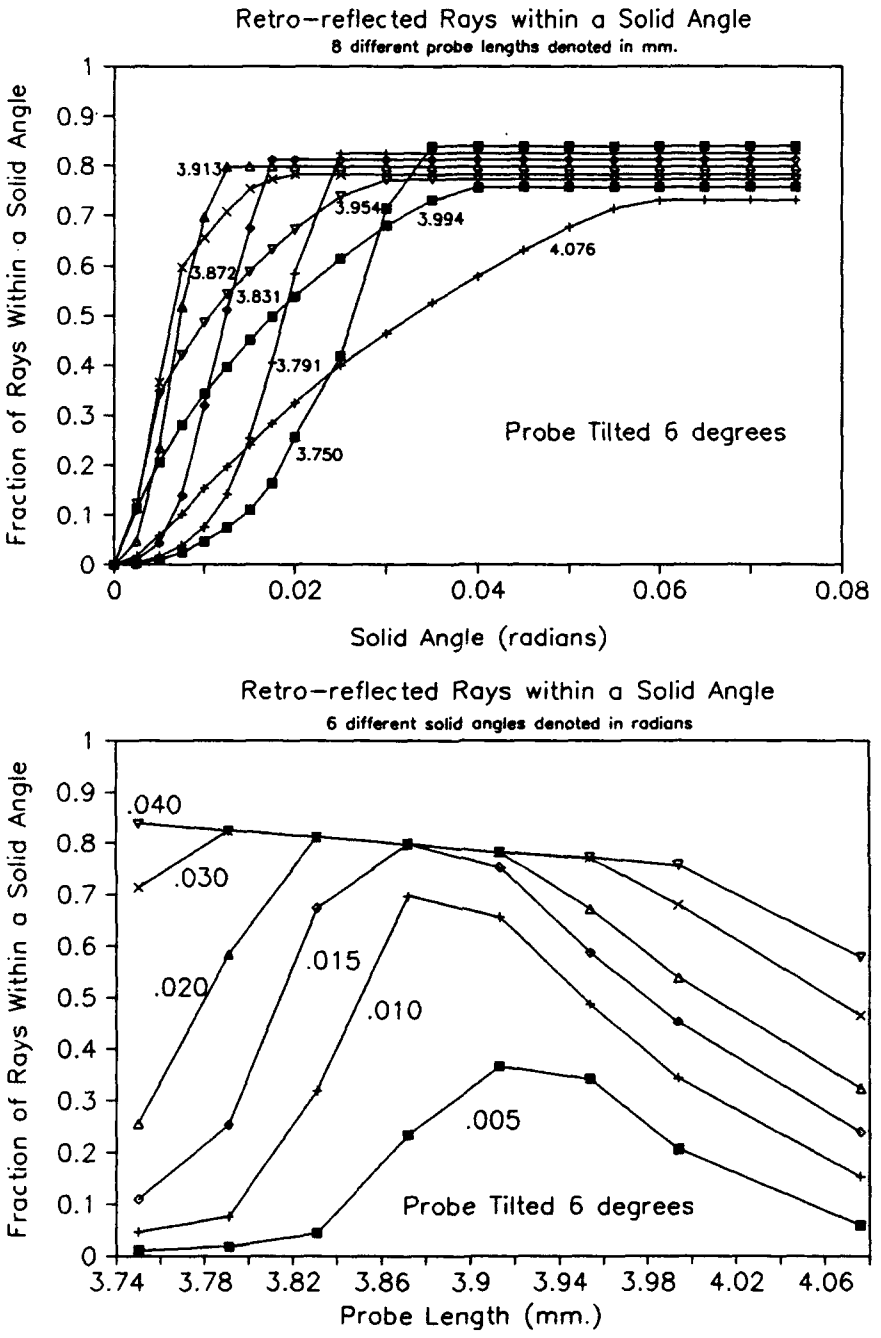

Fig. 4.3 Retroreflected beam divergence for the case of a 6° probe tilt.

5 CARBON/DIAMOND ABLATION TESTS IN A HOT PLASMA

5.1 Introduction

In order to conduct preliminary tests of Diamond versus Carbon pellet ablation in an actual plasma, a prototype pellet injector was constructed and taken to the University of Wisconsin, in Madison, Wisconsin. There 0.6 mm laser-cut cylindrical diamonds (and/or graphite cylinders) were launched at 400-500 m/sec into the Madison Symmetric Torus (MST) reversed field pinch, a large plasma device with an energetic, long-lived plasma. Substantial differences, seen photographically, between the diamond and carbon pellet tracks indicate a significantly reduced ablation rate for the diamond pellets. For reference purposes, similar size frozen hydrogen pellets were also launched into the same plasma.

5.2 Compact Light-Gas Gun Injector

A simple sliding-breech loader mechanism was constructed to allow up to 0.6 mm diameter pellets to be inserted into firing position, in front of a fast opening (and closing) hydrogen gas valve, which then accelerates the pellet down a 30 cm long stainless steel barrel. A $1\,cm^3$ hydrogen gas reservoir at a fill pressure of 1100 psi provides the gas pulse, which is focussed (in a non-optimized manner) onto the pellet. The gas pulse is applied over a 100-200

μsec period by the opening and closing of an electromagnetically-driven, fast-acting, patented Los Alamos fast gas puff valve. The valve technology was originally developed in the CTR-3 plasma group for application on end-plug fuelling of a linear theta-pinch in 1979, and a US patent #4344449, Aug. 17, 1982, was issued to Jim Meyer of Los Alamos. We have obtained one valve and spare parts from LANL. The completed injector and the box of seven diamond pellets are shown in Fig. 5.1. The valve is triggered by a krytron-driven ruby-laser power supply and capacitor, providing a 2.0 kV voltage pulse to a spiral-wound coil in the gas valve, carrying a 6 kA current pulse that causes a magnetic field to accelerate the valve stem, forcing it open. Compression of a nonlinear gas spring returns the valve to its closed position.

Tests of the gun in the open atmosphere, yielded pellets travelling at approximately 300 m/sec. When the gun was integrated with its two-part vacuum system (a low pressure rough pump and surge tank near the barrel, and a high vacuum (turbo-pumped) section isolated by a 2-meter flight tube), the velocity improved to 400-500 m/sec, dependent on the pellet mass. To conserve the number of laser-cut diamonds that were obtained (only seven), all lab bench testing was conducted with metal or graphite pellets, while the system was in Seattle. Pellet velocities were directly measured by observing the timing of interrupted light signals from a He-Ne laser and fast photodiode pairs.

5.3 Pellet/Plasma Test Results

During a two-week period in August 1991, the gun and equipment were installed on the MST device in Wisconsin. The completed installation is shown in Figure 5.2, with four different views of the apparatus, next to the relatively large MST plasma torus. Pumping facilities to remove the unwanted gas load from the light gas gun were provided by the MST group. A four-shot cryogenic hydrogen pellet injector, which was also undergoing initial testing during the same run, was used for the reference hydrogen pellet injection.

After installation of the injector system at Madison, and mounting of appropriate optical monitors (imagery and light diode sensors), the first pellet/plasma shots were conducted using graphite pellets, ranging in length from 0.75 mm to 3.0 mm. A typical 400 m/sec, 2 mm long x 0.6 mm dia. graphite pellet ablation track ablating in a Helium target plasma is shown in Fig. 5.3. The pellet crossed the entire plasma, with little deflection, although it clearly shows fragments breaking away from the main body of the track as it crosses the plasma. These tiny fragments all curve to the right in the picture, due to a rocket-effect caused by differential

ablation of the pellet(s) being bombarded preferentially from the electron drift direction. The bright spot at the top of the photo is due to Helium light emission from a gas puff fuelling valve located on the inner, lower half of the plasma torus, and is not associated with the graphite pellet striking the back wall of the vessel.

As a comparison, two hydrogen pellets, viewed from above and injected at 800 m/sec are shown in Fig. 5.4. The scales are similar to Fig. 5.3, and show an ablation track that is much wider and more diffuse than in the case of carbon (graphite). The pellets also suffered a greater deflection in the electron drift direction, and may have actually struck the bottom of the vacuum vessel.

An important result from this experiment is that launching diamonds is not so easy as graphite, at least in the apparatus used in this test. Seven diamond pellets were attempted, but only two fragmented diamonds were observed entering the plasma. Severe difficulties with the diamond jamming, and evidently breaking (or spallating) in the gun breech were encountered, as the gun was fired. It was noted that the actual size of the diamond cylinders (slightly conically shaped due to the laser-cutting fabrication process) were 0.02 mm larger in diameter than the graphite, while also being shorter than most of the graphite pellets we launched. On some shots the diamonds were actually recovered in the breech mechanism. This was first realized as a scratch when sliding open the bronze/stainless steel breech mechanism, or when the next graphite shot would fail to be seen on the velocity monitor, because it was blocked by a jammed diamond. The use of a sabot, as planned on the TIP experiment, should solve these problems.

The diamonds showed the thinnest ablation track that was observed, compared to hydrogen, lithium, or graphite pellets. A diamond track (corresponding to approximately 30% of the original pellet) from a diamond that made it into the plasma at 400 m/sec is shown in Fig. 5.5. It had a blueish-white tint, and was quite dim, with few signatures on other plasma-related monitors, such a CIII, CIV, or CV emission lines. Unfortunately because the mass of this pellet is unknown, a quantitative comparison cannot be made, although the diamond impact on other plasma parameters was minimal (to nonexistent). During this run, the plasma density interferometer was not functioning, hence the basic plasma density could only be inferred from bremsstrahlung measurements.

5.3.1 Conclusions of the Diamond Ablation Test

The difficulties encountered injecting diamond pellets supports the design for the TIP projectile, in which the diamond encased probe will be held by a sabot during the acceleration through the two-stage light gas gun. The pellet injector used in the diamond ablation study will be similarily modified to permit reliable diamond injection into the MST plasma.

The qualitative results of the diamond ablation study are very promising. The diamond ablation track is both thinner and emits less light than the ablation tracks from the carbon pellets. When the diamond pellets were injected, no large effects were seen on other plasma related monitors, although at the time of the tests the plasma density interferometry system on MST was not operational.

To obtain a quantitative measurement of the diamond ablation rates, further tests will be conducted when the MST interferometry system is operational.

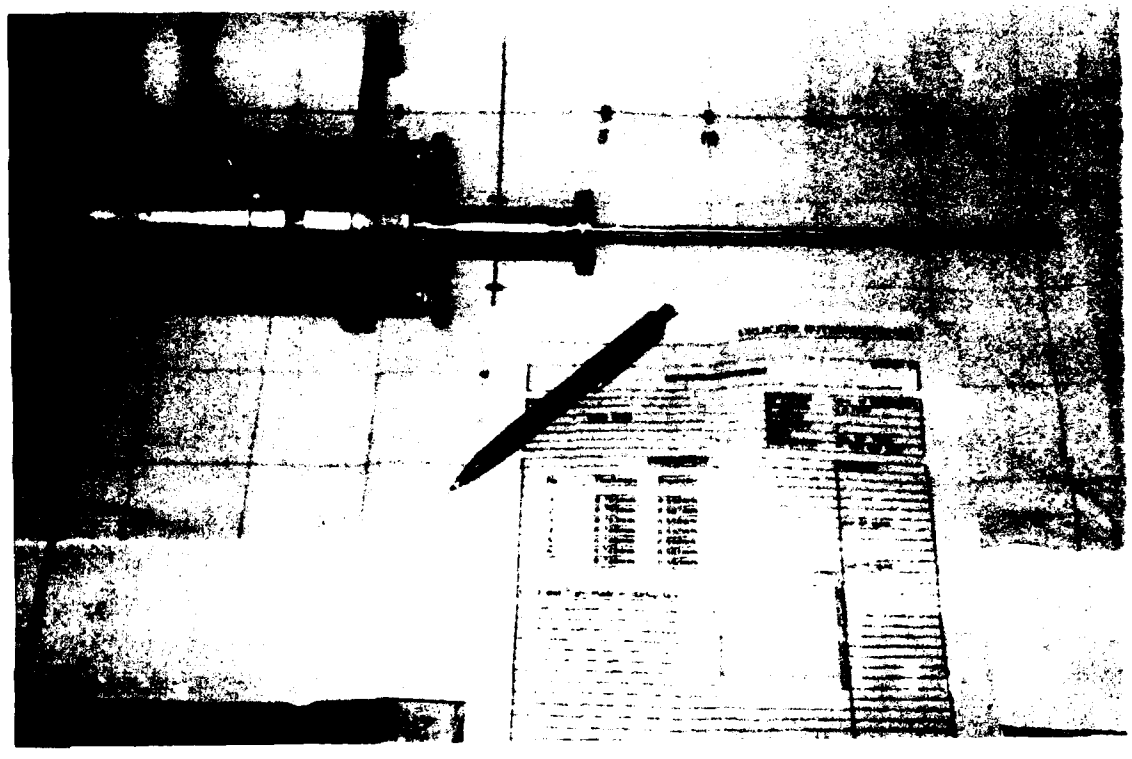

Fig. 5.1 Single-shot gas gun used for prototype experiments, made at the University of Washington, and used at the University of Wisconsin, including electromagnetic gas valve on left, loading mechanism, and exposed 0.6 mm i.d. barrel. Also in the photo is a pencil and box with seven test diamonds.

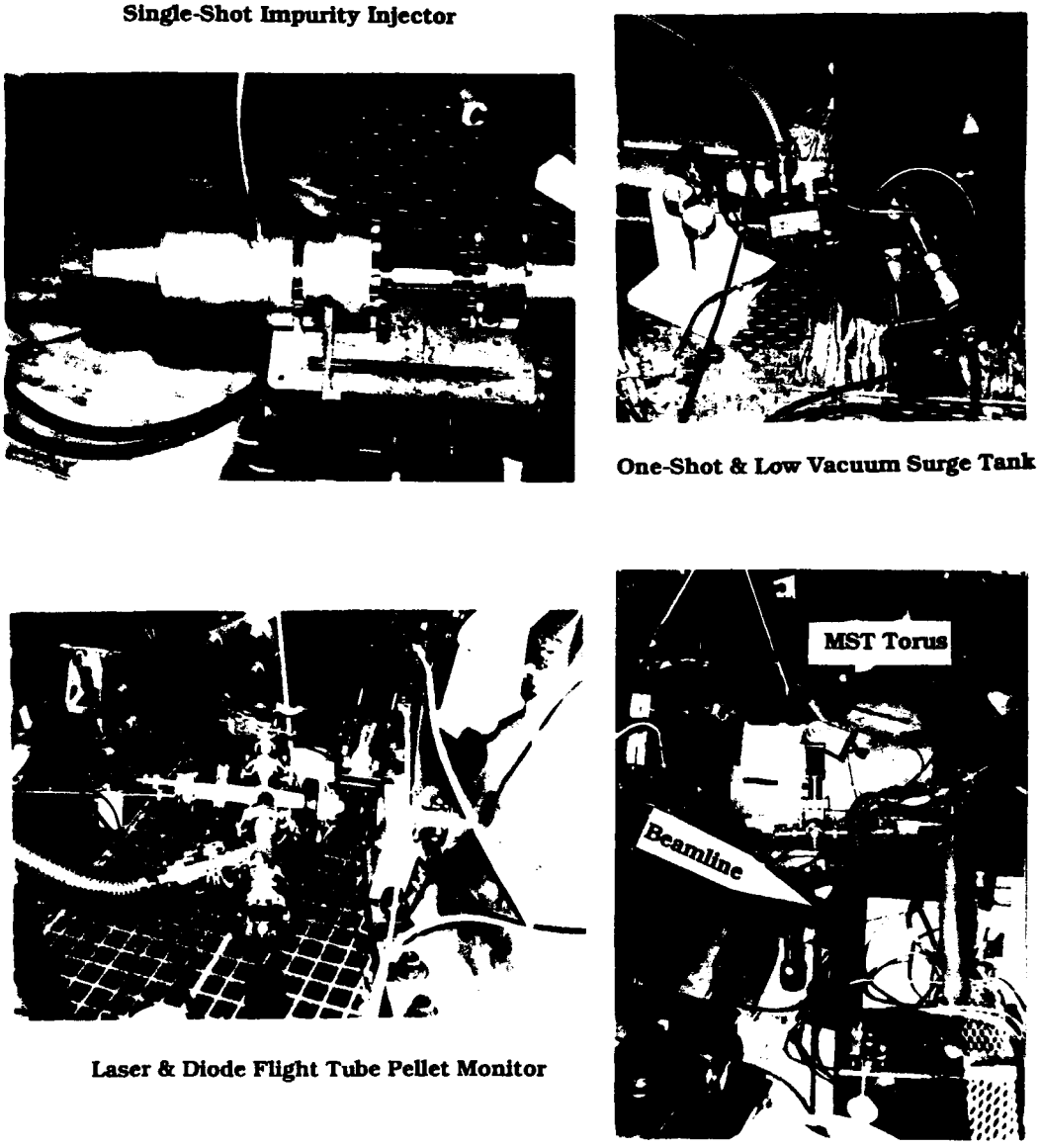

Fig. 5.2 (a) Close-up of installed gun, with 7 kA feed cable and high pressure hydrogen line; (b) Light-gas gun mounted on low-pressure surge tank, with high pressure hydrogen gas bottle nearby; (c) "front-end" differentially pumped section, with pellet guide tube entering from left, and plasma torus seen on right, after vacuum cross (for velocity measurement via laser/diode pair) and isolation gate valves; and (d) Photo along installed "beam-line", which isolates the high pressure gas surge from the high vacuum required in the plasma torus.

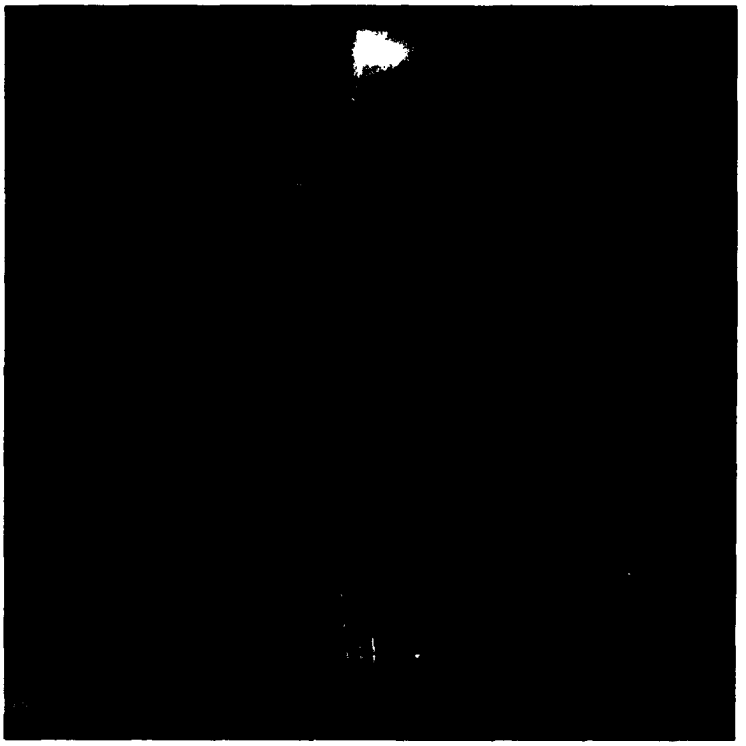

Fig. 5.3 Large Graphite pellet (0.55 mm x 2.0 mm), viewed from above, launched at 400 m/s from the outside midplane of the MST plasma. It fully penetrates the $n_e \sim 10^{13} cm^{-3}, T_e \sim 200 eV$ plasma, while small fragments break off and are accelerated to the right by an asymmetric energy flux causing differential ablation and "rocketing" of the plasma. Curvature of the track is in the electron drift direction.

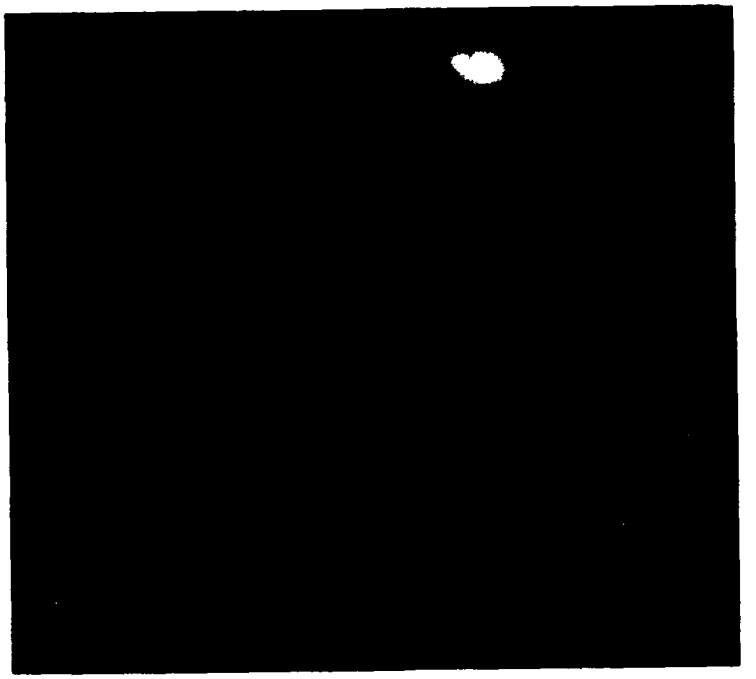

Fig. 5.4 Two hydrogen pellets (each containing $\leq 6x10^{19}$ H atoms) are seen crossing $\sim \frac{3}{4}$ of the 1 meter diameter MST plasma. The bright pink spot at the upper right is due to gas puff refueling of the plasma throughout the discharge by a puff valve on the lower inner wall of the torus.

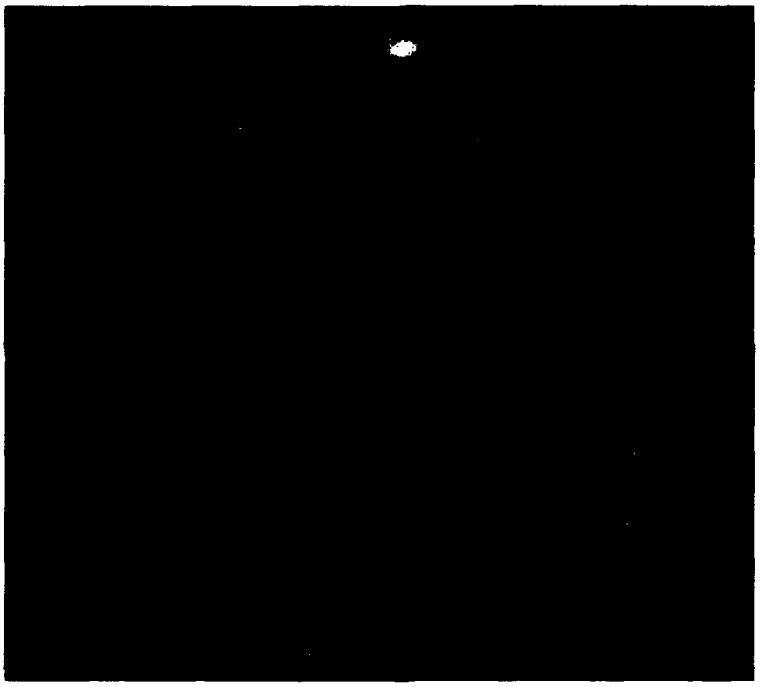

Fig. 5.5 Diamond pellet as seen from above by an unfiltered, open-shutter 35 mm camera, using a reenterent fisheye lens. The diamond enters from the outside midplane of the photo. The extremely narrow track has a blue-white color, unlike either the graphite or hydrogen pellet tracks.